nature geoscience

ARTICLES

PUBLISHED ONLINE: 25 SEPTEMBER 2017 | DOI: 10.1038/NGEO3032

Magmatic pulse driven by sea-level changes associated with the Messinian salinity crisis

Pietro Sternai[1]*, Luca Caricchi[1], Daniel Garcia-Castellanos[2], Laurent Jolivet[3†], Tom E. Sheldrake[1] and Sébastien Castelltort[1]

Between 5 and 6 million years ago, during the so-called Messinian salinity crisis, the Mediterranean basin became a giant salt repository. The possibility of abrupt and kilometre-scale sea-level changes during this extreme event is debated. Messinian evaporites could signify either deep- or shallow-marine deposits, and ubiquitous erosional surfaces could indicate either subaerial or submarine features. Significant and fast reductions in sea level unload the lithosphere, which can increase the production and eruption of magma. Here we calculate variations in surface load associated with the Messinian salinity crisis and compile the available time constraints for pan-Mediterranean magmatism. We show that scenarios involving a kilometre-scale drawdown of sea level imply a phase of net overall lithospheric unloading at a time that appears synchronous with a magmatic pulse from the pan-Mediterranean igneous provinces. We verify the viability of a mechanistic link between unloading and magmatism using numerical modelling of decompression partial mantle melting and dyke formation in response to surface load variations. We conclude that the Mediterranean magmatic record provides an independent validation of the controversial kilometre-scale evaporative drawdown and sheds new light on the sensitivity of magmatic systems to the surface forcing.

Local- or regional-scale magmatic activity has been linked to modifications of the environmental conditions, either by driving climate changes[1] or in response to surface load variations due to glacio-eustatic changes[2–7]. The Mediterranean Messinian salinity crisis (MSC) occurred between ~5.97–5.33 Myr ago (Ma; ref. 8) due to the temporary closure of the Strait of Gibraltar, resulted in the formation of thick evaporitic layers in the deep basin and inland[9–11], and involved a combination of environmental and eustatic changes that may also have influenced the regional magmatism. However, although the occurrence of an intra-MSC sea-level lowering is widely accepted today[12], questions remain about the magnitude and modalities of the desiccation[13,14]. This controversy stems from the discovery of deep fluvial incision extending from the Mediterranean into the Eurasian and African continents[15], leading to discussions regarding the shallow or deep marine deposition of the Messinian evaporites[16,17].

Surface load variations and the igneous record

To investigate the potential impact of the MSC on Mediterranean magmatism, we calculate the overall surface load variations associated with sea-level and water-density changes as well as the formation of salt deposits (Methods). We first test the scenario proposed by ref. 18 (Fig. 1a), based on both direct and geophysical observations and conveniently covering the entire Mediterranean. According to this model, lithospheric loading occurs during the early MSC due to increased water salinity and limited evaporative drawdown and salt deposition (Fig. 1b). The contribution to surface load variations by salt deposition should be reduced by 50% to 75% to account for the interleaved sediment[18]. As a result, during the late-MSC, the unloading due to the drawdown overcomes the loading by increased water density and salt deposition by up to ~15 and ~10 MPa, on average, in the eastern and western Mediterranean, respectively. These estimates are highly conservative as they do not account for erosion both onshore and on present-day shelves and slopes[15,19], which implies additional lithospheric unloading synchronous and prior to the evaporative drawdown of the brine surface[20].

To compare these results with regional magmatic trends we count the number of intrusive and effusive events from the pan-Mediterranean igneous provinces during the Neogene period, based on published igneous mineral ages (Methods and Supplementary Table 1). During the late-MSC a gross but concrete magmatic pulse, significant at the ~95% confidence level, is observed (Fig. 1c,d). Such a late-MSC peak magmatism is widespread but particularly concerns the eastern Mediterranean, where the salt is distributed over a larger area and, according to the reference MSC scenario[18], the drawdown is more significant (Fig. 1a). The short-lived late-MSC increase in magmatism, in addition, cannot be justified by significant changes of overall geodynamics[21] (Methods and Supplementary Fig. 1). The correspondence between the recognized magmatic pulse and the estimated net lithospheric unloading during the late-MSC is striking (Fig. 1a–c), suggesting that the intra-MSC drawdown enhanced active magmatic processes, which include partial mantle melting by adiabatic decompression and dyke formation[22–24] (more details below).

We also explore two alternative loading/unloading scenarios (Supplementary Fig. 2). The first involves an earlier and shorter timing for the intra-MSC drawdown and shallow-marine salt deposition, as suggested by seismic surveys and field observations from the Gulf of Lions, Italy and Turkey[25]. The second assumes the deep-water formation of the Messinian evaporites in the absence of significant drawdown[13,14]. In the first case, considerable net average lithospheric unloading still occurs and is largely synchronous with the magmatic pulse. Conversely, the deep-water scenario for the formation of the Messinian evaporites implies net average

[1]Department of Earth Sciences, University of Geneva, CH-1205 Geneva, Switzerland. [2]Instituto de Ciencias de la Tierra Jaume Almera, ICTJA-CSIC, 08028 Barcelona, Spain. [3]Intitut des Sciences de la Terre d'Orléans, University of Orléans, 45100 Orléans, France. [†]Present address: University Pierre et Marie Curie (UPMC-Paris VI), 75005 Paris, France. *e-mail: pietro.sternai@unige.ch

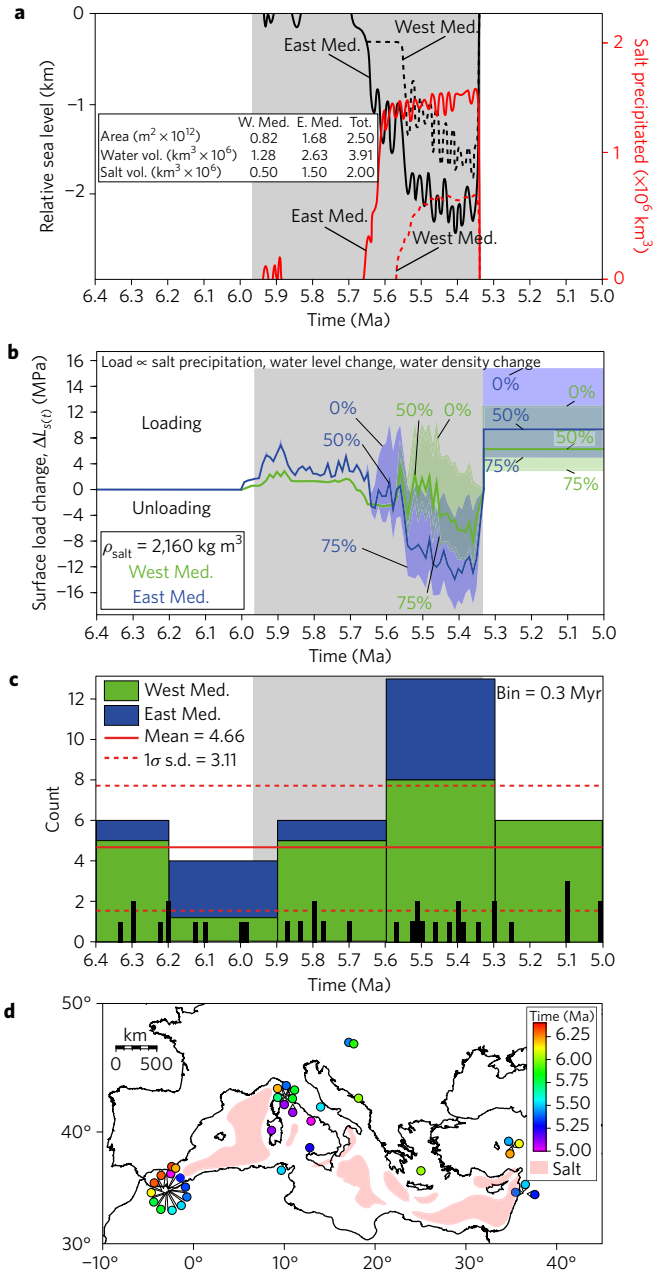

Figure 1 | Distribution of Mediterranean magmatic minerals dated between 5 and 6.4 Ma and surface load variation estimates by the reference MSC scenario. a, Relative sea level and salt precipitation (ref. 18), the inset provides values to convert salt volumes into average thickness. **b**, $\Delta L_{s(t)}$ (that is, surface load changes) estimated from the curves in **a** and Supplementary Fig. 5. The 0%, 50% and 75% curves show $\Delta L_{s(t)}$ after reducing the salt volume by that amount to account for interleaved sediments. **c**, Mineral age histogram (black bars show the distribution). Red lines show the time-averaged count and the 1σ s.d. **d**, Sample ages and locations and distribution of major salt deposits. The grey bar in **a**–**c** highlights the MSC.

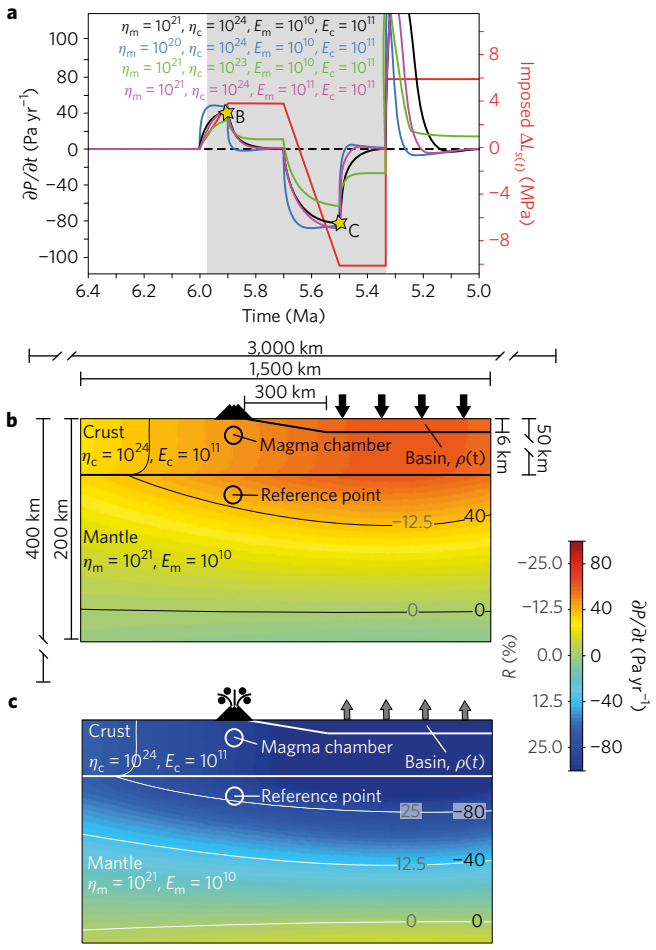

Figure 2 | Pressure and melt production change rate at depth in response to the MSC-related surface load variations. a, The red curve shows the imposed surface load variations, mimicking the MSC-related surface load change, $\Delta L_{s(t)}$ (Fig. 1b). The other curves show the parametric study on the viscosities, η_c and η_m, and elastic moduli, E_c and E_m, of the upper and lower layers (analogue for the crust and mantle, respectively). Curves are computed at the reference points shown in **b** and **c**. The grey bar highlights the MSC. **b**,**c**, $\partial P/\partial t$ and $R_{(t)} = (1/\rho_m g V_y)(\partial P/\partial t)$ (see Methods) at the time step shown by the stars in **a**. $\Delta L_{s(t)}$ is imposed by modulating the density of the material within the basin-like structure.

lithospheric loading during the entire MSC, which is, based on the principles that we explore hereafter, at odds with the recognized magmatic trends.

Effects on magma production and dyke formation

The following quantitative assessments inherent to the geodynamic context provide independent support for the existence of a causative link between the estimated MSC-related surface load variations and the regional magmatic trends. Since at least the Oligocene epoch, the Africa–Eurasia convergence and rollback of subducting slabs characterize the Mediterranean geodynamics[21], while partial melting by adiabatic decompression of hydrated mantle rocks across extensional back-arc domains controls the bulk of the regional magmatism[22–24] (see also Methods). Back-arc spreading occurred at rates up to a few cm yr^{-1} (ref. 21), causing parcels of mantle to flow upwards at similar rates. Such upwelling leads to a background geodynamic decompression of rising mantle rocks on the order of hundreds of Pa yr^{-1}. Our geodynamic numerical models (Methods) suggest that pressure changes at depth in response to the MSC-related surface load variations vary on the order of tens of Pa yr^{-1} and may reach up to one order of magnitude higher during extreme events (Fig. 2). These values also apply to modelled pressure changes below the edges of the basin-like structure, representative of regions where most observations reporting on the Mediterranean magmatism are found (Fig. 1 and Supplementary Table 1). Hence, MSC-related surface load variations would modify the background geodynamic depressurization rates by a minimum amount of ~10%.

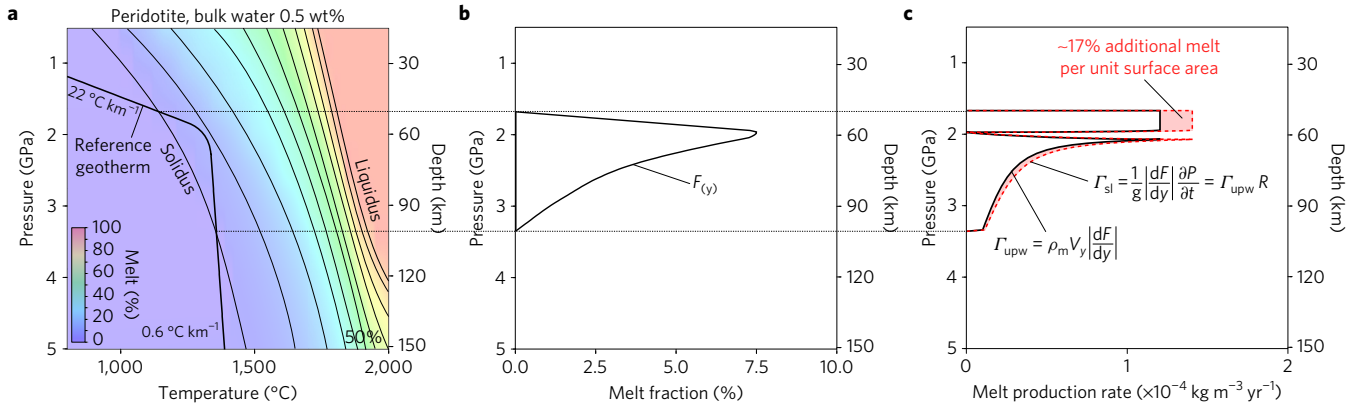

Figure 3 | Partial melting of partially hydrated mantle rocks modulated by surface unloading. a, Equilibrium melt percentage of a peridotite (calculations based on MELTS, ref. 26). Initial rock composition: SiO_2, 45.47%; TiO_2, 0.11%; Al_2O_3, 4%; Fe_2O_3, 0.585%; Cr_2O_3, 0.68%; FeO, 6.696%; MgO, 38.53%; CaO, 3.59%; MaO, 0.31%; H_2O, 0.5%. The thick black line shows a reference geotherm. **b**, Melt fraction versus depth/pressure for the reference geotherm. **c**, Melt production rate versus depth/pressure at equilibrium conditions (black curve) and after correction by R in Fig. 2c, along the vertical through the reference point (dashed red curve). We assume uniform and constant $\rho_m = 3{,}300\ kg\ m^{-3}$ and $V_y = -1\ cm\ yr^{-1}$, where the minus sign indicates upwelling, also see Methods.

Assessing the corresponding effects on the volumes of magma produced is difficult, especially because quantitative constraints on the Mediterranean thermo-chemical structure during the MSC are lacking. However, assuming uniform and constant mantle upwelling and density, the modulation in melt production rate due to surface load changes scales linearly with their modification of the pressure change rate in the mantle (see Methods, equations (4)–(6)). In Fig. 3a, we consider an equilibrium continental geothermal structure and a parameterization for partial mantle melting as a function of pressure and temperature[26]. In Fig. 3b, we show the degree of partial melting at depth and, in Fig. 3c, the melt production rate at equilibrium conditions is increased by an amount equivalent to that associated with the relative modification of the depressurization rates by the MSC-related surface unloading shown in Fig. 2c, along the vertical through the reference point. We found an increase in the depth-integrated melt production rate (that is, additional melt) per unit surface area by ~17% during the unloading phase of the reference MSC scenario. In the case of surface unloading where the depth-integrated amount of melts measures 6 km, this translates into the approximate production of an additional km^3 of melts for each km^2 subject to unloading, only due to the surface forcing. This estimate is conservative, considering that the portion of partially molten Mediterranean mantle is in many places thicker than 6 km (ref. 27) and that the Messinian geothermal structure of the Mediterranean back-arc regions was probably hotter than the equilibrium state considered here.

The rate of upward percolation of the mantle melts with respect to the solid matrix determines the time lag between the production and the eruption/emplacement of magma. This quantity primarily depends on the lithosphere and asthenosphere permeability. Because the igneous activity of the magmatic provinces in Fig. 1d was initiated prior to the MSC[22–24,28], one can assume that the vertical connections of channels along the solid matrix grain boundaries were already established. Under this assumption, and according to the porous flow model proposed by refs 29,30, the vertical migration velocity of the magma varies on the order of tens of $m\ yr^{-1}$, which implies that a considerable amount of newly produced magma would reach shallow crustal reservoirs (or be erupted) within a few tens of thousands of years after the MSC-related unloading phase. However, such a time lag can increase considerably if, for instance, the deformation and collapse of the solid matrix is not sufficiently rapid to provide the vertical connections of channels along grain boundaries, or depending on the viscosity and density of the melts with respect to those of the matrix[30].

At shallower levels, the overpressure within crustal magma reservoirs, $\Delta P_{ch} = P_{ch} - P_r$ (where P_{ch} is the pressure within the reservoir and P_r is the remote lithostatic stress), affects the frequency of volcanic eruptions[3]. Increased magma fluxes can increase P_{ch}, while surface load variations control the tensile deviatoric stresses required to dilate fractures by modulating P_r, inhibiting or facilitating dyke formation when loading or unloading, respectively, take place. According to the model presented in ref. 3 (Methods), the elastic instantaneous response of a magmatic system is proportional to the rates of surface load changes. We remark that, regardless of the MSC scenario that is considered, MSC-related loading/unloading rates (for example, Fig. 1b and Supplementary Fig. 2) are considerably higher than during Quaternary glacio-eustatic changes, which have been proven capable of affecting the Mediterranean volcanism[7].

In Fig. 4a, we show the computed overpressure time history within a hypothetical magma chamber at 20 km depth based on the analytical framework provided by ref. 3 (see Methods, equations (7) and (8)) and the pressure changes at depth from our geodynamic models (Fig. 2). Such a calculation shows that the estimated surface unloading related to MSC scenarios involving a kilometre-scale sea-level drawdown (for example, Fig. 1a,b) can enhance the overpressure within the magma chamber, thereby increasing the likelihood of dyke formation. This effect would be even more pronounced if the drop in sea level was of similar magnitude but occurred faster (for example, the MSC scenario in Supplementary Fig. 2a,b), for the rate of change of surface load is the leading-order factor controlling the magmatic response in terms of dyke formation. It is also noteworthy that, besides the effects on ΔP_{ch} due to modulations of P_r, the MSC-related surface loading or unloading may respectively lead to horizontal compressional or extensional deviatoric stresses at crustal levels (Fig. 4b,c and Supplementary Fig. 3), which can further inhibit/help the nucleation and propagation of dykes[31]. Eruptions by overpressure and dyke formation due to the MSC-related surface load variations should be delayed by ~10 kyr because of the partly viscous rock rheology[3]. Yet, such a delay is short enough to allow us to relate the observed regional magmatic pulse to the net average unloading of the Mediterranean lithosphere during the late-MSC.

Increased magmatic activity appears associated with melting of ice sheets and erosion across thickened continental lithospheres[3,4,6]. The MSC implies a similar surface forcing, but on the Mediterranean basin, which is atop of a lithosphere that has been subject to

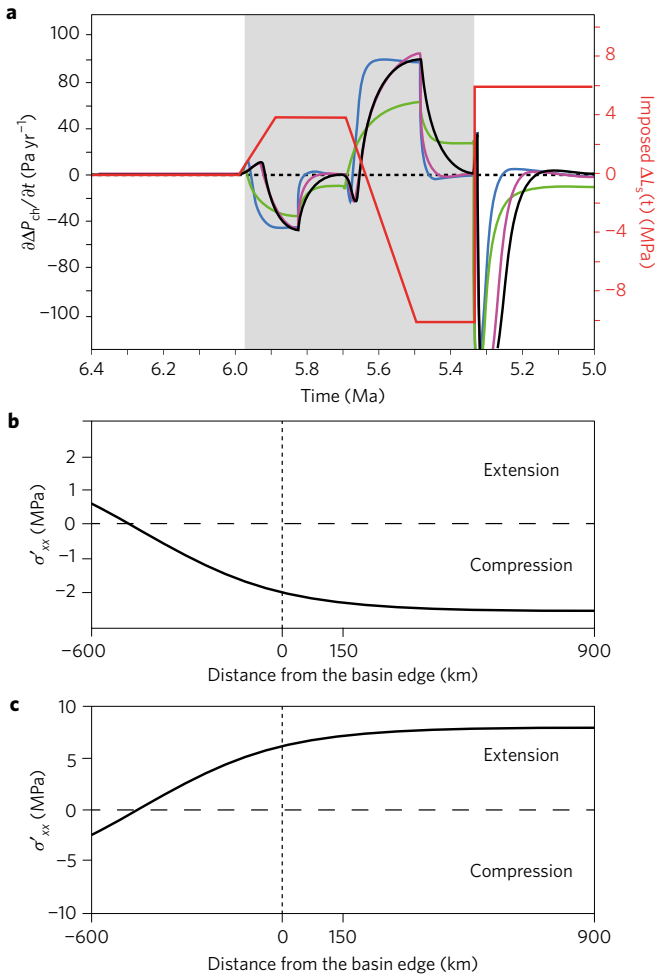

Figure 4 | Overpressure and deviatoric horizontal stresses for the geodynamic model in Fig. 2. a, Temporal variations of the overpressure within a hypothetical magma chamber at 20 km depth, above the reference point (shown in Fig. 2b,c). The colour scheme is the same as in Fig. 2a. **b**,**c**, Deviatoric horizontal stress, σ'_{xx}, at 20 km depth for the model time steps shown in Fig. 2b,c, respectively. The horizontal distance is relative to the edge of the basin-like structure (vertical dashed line). Note that crustal levels below and nearby the basin-like structure are subject to slight horizontal compression and extension during the loading and unloading phase, respectively.

widespread thinning and warming since at least the Oligocene[21]. We thus propose that the net mean lithospheric unloading during the late-MSC is a likely cause behind the synchronous pulse of the Mediterranean magmatism derived from available geochemical data. Given the volume of Messinian evaporites, however, only scenarios involving a kilometre-scale sea-level fall[9,18,25] can explain the magmatic pulse by the mechanisms proposed here. Although this does not rule out the precipitation of the Messinian evaporites under a significant water column, it does point towards their formation in a partially desiccated Mediterranean basin. Our study also provides support for the vision that the melting of the solid Earth is highly sensitive to the surface forcing[4–6], greatly advancing ongoing debates[5,32]. More data and work in this novel direction are warranted and could, for instance, allow one to distinguish between either multiple short intra-MSC desiccations[33] or a long-lasting shallow Mediterranean–Atlantic connection[34]. In any case, we anticipate that the environmental changes associated with the MSC had far bigger effects on the Mediterranean magmatism than have been proposed thus far.

Methods

Methods, including statements of data availability and any associated accession codes and references, are available in the online version of this paper.

Received 2 February 2017; accepted 23 August 2017; published online 25 September 2017

References

1. Jicha, B., Scholl, D. W. & Rea, D. Circum-Pacific arc flare-ups and global cooling near the Eocene–Oligocene boundary. *Geology* **37,** 303–306 (2009).
2. Jull, M. & McKenzie, D. The effect of deglaciation on mantle melting beneath Iceland. *J. Geophys. Res.* **101,** 21815–21828 (1996).
3. Jellinek, A. M., Manga, M. & Saar, M. O. Did melting glaciers cause volcanic eruptions in eastern California? Probing the mechanics of dike formation. *J. Geophys. Res.* **109,** B09206 (2004).
4. Huybers, P. & Langmuir, C. Feedback between deglaciation, volcanism, and atmospheric CO_2. *Earth Planet. Sci. Lett.* **286,** 479–491 (2009).
5. Crowley, J. W., Katz, R. F., Huybers, P., Langmuir, C. & Park, S.-H. Glacial cycles drive variations in the production of oceanic crust. *Science* **347,** 1237–1240 (2015).
6. Sternai, P., Caricchi, L., Castelltort, S. & Champagnac, J.-D. Deglaciation and glacial erosion: a joint control on magma productivity by continental unloading. *Geophys. Res. Lett.* **43,** 1–10 (2016).
7. McGuire, W. J. *et al*. Correlation between rate of sea-level change and frequency of explosive volcanism in the Mediterranean. *Nature* **389,** 473–476 (1997).
8. Gautier, F., Clauzon, G., Suc, J. P., Cravatte, J. & Violanti, D. Age et durée de la crise de salinité messinienne. *C. R. Acad. Sci.* **318,** 1103–1109 (1994).
9. Hsü, K. J., Ryan, W. B. & Cita, M. Late Miocene desiccation of the Mediterranean. *Nature* **242,** 240–244 (1973).
10. Ogniben, L. Petrografia della Serie Solfifera Siciliana e considerazioni geologiche relative. *Mem. Descr. Carta Geol. Ital.* **22,** 1–275 (1957).
11. Perrodon, A. Etude géologique des bassins néogènes sublittoraux de l'Algérie occidentale. *Bull. Serv. Carte Géol. Algér* **12,** 328 (1957).
12. Clauzon, G., Suc, J. P., Gautier, F., Berger, A. & Loutre, M. F. Alternate interpretation of the Messinian salinity crisis: controversy resolved? *Geology* **24,** 363–366 (1996).
13. Roveri, M. *et al*. Dense shelf water cascading and Messinian canyons: a new scenario for the Mediterranean salinity crisis. *Am. J. Sci.* **314,** 751–784 (2014).
14. Lugli, S., Manzi, V., Roveri, M. & Schreiber, B. The deep record of the Messinian salinity crisis: evidence of a non-desiccated Mediterranean Sea. *Palaeogeogr. Palaeoclimatol. Palaeoecol.* **297,** 83–99 (2015).
15. Urgeles, R. *et al*. New constraints on the Messinian sealevel drawdown from 3D seismic data of the Ebro Margin, western Mediterranean. *Basin Res.* **23,** 123–145 (2011).
16. Roveri, R. *et al*. The Messinian salinity crisis: past and future of a great challenge for marine sciences. *Mar. Geol.* **352,** 25–58 (2014).
17. Hsü, K. J., Cita, M. & Ryan, B. in *Initial Reports of the Deep Sea Drilling Project* Vol. 13 (eds Ryan, W. F. B. & Hsü, K. J. *et al*.) 1203–1231 (US Government Printing Office, 1973).
18. Ryan, W. B. Modeling the magnitude and timing of evaporative drawdown during the Messinian salinity crisis. *Stratigraphy* **5,** 227–243 (2008).
19. Ryan, W. B. & Cita, M. B. The nature and distribution of Messinian erosional surfaces—indicators of a several-kilometer-deep Mediterranean in the Miocene. *Mar. Geol.* **27,** 193–230 (1978).
20. Ryan, W. B. Geodynamic responses to a two-step model of the Messinian salinity crisis. *Bull. Soc. Géol. Fr.* **182,** 73–78 (2011).
21. Jolivet, L., Augier, R., Robin, C., Suc, J. P. & Rouchy, J. M. Lithospheric-scale geodynamic context of the Messinian salinity crisis. *Sediment. Geol.* **188–189,** 9–33 (2006).
22. Duggen, S., Hoernle, K., van den Bogaard, P. & Harris, C. Magmatic evolution of the Alboran region: the role of subduction in forming the western Mediterranean and causing the Messinian Salinity Crisis. *Earth Planet. Sci. Lett.* **218,** 91–108 (2004).
23. Jolivet, L. & Brun, J.-P. Cenozoic geodynamic evolution of the Aegean. *Int. J. Earth Sci.* **99,** 109–138 (2010).
24. Serri, G. F., Innocenti, F. & Manetti, P. Geochemical and petrological evidence of the subduction of delaminated Adriatic continental lithosphere in the genesis of the Neogene–Quaternary magmatism of Central Italy. *Tectonophysics* **223,** 117–147 (1993).

25. Bache, F. *et al*. A two step process for the reflooding of the Mediterranean after the Messinian Salinity Crisis. *Basin Res.* **24,** 125–153 (2012).
26. Ghiorso, M. S., Hirschmann, M. M., Reiners, P. W. & Kress, V. C. The pMELTS: a revision of MELTS for improved calculation of phase relations and major element partitioning related to partial melting of the mantle to 3 GPa. *Geochem. Geophys. Geosyst.* **3,** 1–35 (2002).
27. Tumanian, M., Frezzotti, M. L., Peccerillo, A., Brandmayr, E. & Panza, G. Thermal structure of the shallow upper mantle beneath Italy and neighbouring areas: correlation with magmatic activity and geodynamic significance. *Earth-Sci. Rev.* **114,** 369–385 (2012).
28. Jolivet, L. *et al*. Ductile extension in alpine Corsica. *Geology* **18,** 1007–1010 (1990).
29. Turcotte, D. L. & Schubert, G. *Geodynamics* (Cambridge Univ. Press, 2002).
30. Turcotte, D. L. & Ahern, J. L. A porous flow model for magma migration in the asthenosphere. *J. Geophys. Res.* **83,** 767–772 (1978).
31. Rubin, A. M. Tensile fracture of rock at high confining pressure: implications for dike propagation. *J. Geophys. Res.* **98,** 15919–15935 (1993).
32. Olive, J.-A. *et al*. Sensitivity of seafloor bathymetry to climate-driven fluctuations in mid-ocean ridge magma supply. *Science* **350,** 310–313 (2015).
33. Gargani, J. & Rigollet, C. Mediterranean sea level variations during the Messinian salinity crisis. *Geophys. Res. Lett.* **34,** 10 (2007).
34. Garcia-Castellanos, D. & Villaseñor, A. Messinian salinity crisis regulated by competing tectonics and erosion at the Gibraltar arc. *Nature* **480,** 359–363 (2011).

Acknowledgements

P.S. is grateful to the Swiss NSF for providing funding for this project (Ambizione grant PZ00P2_168113/1). L.C. and T.E.S. were funded by the European Research Council (ERC) under the European Union's Horizon 2020 research and innovation programme (grant agreement No. 677493 — FEVER). D.G.-C. was funded by the MITE CGL2014-59516 (Spanish Government). S.C. was funded by Swiss NSF grant No. 200021–146822. J.-A. Olive is thanked for helpful suggestions regarding Fig. 3 and all related aspects.

Author contributions

P.S. conceived the scientific question, designed and performed the work and wrote the manuscript. L.C. contributed to the conception of the scientific question and helped with the MELTS modelling. D.G.-C. and L.J. provided fundamental insights into the available knowledge about the MSC as well as the Mediterranean geodynamics and magmatism. T.E.S. helped with the statistical treatment of data. S.C. contributed to the conception of the scientific question. All authors contributed to the design of the work and improved the manuscript.

Additional information

Supplementary information is available in the online version of the paper. Reprints and permissions information is available online at www.nature.com/reprints. Publisher's note: Springer Nature remains neutral with regard to jurisdictional claims in published maps and institutional affiliations. Correspondence and requests for materials should be addressed to P.S.

Competing financial interests

The authors declare no competing financial interests.

Methods

Mediterranean geodynamic and magmatic context. The geodynamic and magmatic evolution of the Mediterranean during the Cenozoic era is controlled by the Africa–Eurasia convergence and the associated collisional and subduction dynamics (Supplementary Fig. 1). Since the late Oligocene, the collision between Africa and Eurasia in the Betic cordillera and the Rif as well as in the Hellenides and Taurides constrained the Mediterranean subductions in the east and west, respectively[35]. As a result, rollback of the subducting slabs became predominant and led to the opening of the major back-arc basins that shape the present-day physiography of the Mediterranean: the Alboran Sea, the Liguro-Provençal basin, the Tyrrhenian Sea and the Aegean Sea. During the Messinian, probably due to the narrow space available for slab retreat, limited back-arc extension is observed in the Alboran Sea[36]. Conversely, back-arc extension related to slab rollback developed since the early Miocene epoch in the internal Apennines and the northern Tyrrhenian Sea[37], and progressively migrated eastward through time[38]. Similarly, following the late-Oligocene collisional events, the Aegean back-arc extension migrated regularly southwards due to ongoing rollback of the Hellenic slab[23].

Neogenic magmatic rocks in the westernmost Mediterranean, which provide debated clues on the origins of the MSC[21,22,39], are found onshore and offshore along a NE–SW trending lineament across the Alboran Sea and the western Betics. A transition toward shoshonites and alkali basalts, largely synchronous with the MSC, in particular, is interpreted as the shift from subduction-related to intra-plate magmatism due to slab detachment and associated asthenospheric mantle upwelling and decompression melting[22]. The magmatic activity in the Tyrrhenian Sea accompanies the eastward migration of the back-arc extension[28] and is predominantly characterized by granitoid intrusives and associated volcanic products[24]. Also the Aegean magmatism migrated regularly southwards, following the back-arc extensional domain migration, to reach its present-day position[23]. Despite the unusual range of chemistry and petrology, the overall Aegean picture is compatible with arc and back-arc magmatism[40]. Since the middle Miocene, slab tearing below western Turkey and the associated toroidal and upwelling mantle flow controlled the intense regional tectonics and magmatism[23,41–43]. Thus, the bulk of the late-Cenozoic Mediterranean magmatism appears to be related to decompression partial melting of upwelling mantle rocks due to slab detachment and/or stretching of the upper plate.

Estimates of surface load variations during the MSC. Our reference MSC scenario is provided by ref. 18 (Fig. 1a), which models the magnitude and timing of the sea-level variations, water salinity and salt deposition during the MSC based on the physical laws controlling the water exchange between the Atlantic and the Mediterranean. The volumes of the evaporites and the Mediterranean palaeo-climate and palaeo-hypsometric conditions (as compiled from available data sets[18]) are the primary boundary conditions for this model. We rely on this work to compute the MSC-related surface load variations because of its more realistic hypsometry relative to previous models[44] and because it takes into account the environmental lapse rate, the control by precession cycles on rainfall and river input, and global eustatic changes calibrated on $\delta^{18}O$ data. These models, however, differ in the details but agree on the magnitudes; therefore, we expect that the model by ref. 44 would lead to similar results. The scenario proposed by ref. 25, involving a shorter time lag for the drawdown and evaporites deposition and earlier drawdown with respect to the evaporites deposition[20] based on inshore and offshore observations from the Gulf of Lions, Italy and Turkey, is also considered (Supplementary Fig. 2). Finally, we account for a 'no-drawdown' scenario for the MSC[13,14] by removing the contribution to surface load variations by sea-level changes from the time history proposed by ref. 18.

For each of the three representative scenarios, variations of the surface load with respect to pre-MSC conditions, $\Delta L_{s(t)}$ (Fig. 1b and Supplementary Fig. 2), are computed as:

$$\Delta L_{s(t)} = g(\rho_{w(t)} h_{w(t)} + \rho_s h_{s(t)} - \rho_{w(t_0)} h_{w(t_0)} + \rho_s h_{s(t_0)}) \quad (1)$$

where $\rho_{w(t)}$ is the time-dependent mean water density, ρ_s is the mean salt density (time independent), $h_{w(t)}$ and $h_{s(t)}$ are the time-dependent mean water depth and salt deposit thickness, g is the vertical component of the acceleration due to gravity, and subscript (t_0) indicates quantities at a reference time soon before the onset of the MSC. Assuming that $h_{s(t_0)}$ is zero, equation (1) becomes:

$$\Delta L_{s(t)} = g(\rho_{w(t)} h_{w(t)} + \rho_s h_{s(t)} - \rho_{w(t_0)} h_{w(t_0)}) \quad (2)$$

ρ_s and $\rho_{w(t_0)}$ are set to 2,160 kg m^{-3} and 1,029 kg m^{-3}, respectively. $\rho_{w(t)}$ (Supplementary Fig. 5) is constrained by the salinity changes estimated by ref. 18, and the equation of state for seawater by ref. 45 (the ocean water density calculator available at http://www.csgnetwork.com/water_density_calculator.html was used for this operation). We set $h_{w(t_0)}$ equal to 2,500 m, which is approximately the mean bathymetry of the Mediterranean in the Messinian[46]. $h_{w(t)}$ is obtained by adding to this value the water surface changes (negative for lowering) provided by refs 18,25, whereas it is assumed constant through time for the 'no-drawdown' scenario. $h_{s(t)}$ is constrained by the time history of salt deposition provided by refs 18,25 divided by the area of the Mediterranean basins (Fig. 1a and Supplementary Fig. 2). Note that the volumes of salt deposits are overestimated by not being corrected for the interleaved detritus, and more appropriate values are obtained by applying a reduction by up to 75% (ref. 18). We thus compute envelopes that report on estimates of $\Delta L_{s(t)}$ accounting for a reduction of $h_{s(t)}$ by 0% (that is, no modification of the salt volumes provided by ref. 18), 50% and 75% (Fig. 1b and Supplementary Fig. 2).

Igneous mineral ages compilation and analysis. Volumetric estimates of the magmatic products during the MSC are limited by compromised preservation due to erosion and the Plio-Quaternary tectonics. Instead, the number of volcanic and intrusive events, represented by igneous mineral ages during the time window of interest, is often used as a proxy for local, regional or global magmatic trends[1,7,47,48]. We follow this approach and generate a database of published mineral ages of igneous rocks from the pan-Mediterranean area during the 6.4–5 Ma time window (Supplementary Table 1) based on careful manual literature screening (Fig. 1c,d, a full reference list is provided in the Supplementary Information). Selected units are separated in space and time by at least 10 km and 10 kyr, which enables avoiding bias due to multiple sampling or studies focused on particular events or regions, and a single entry is assigned to each unit. 35 entries compose our database; we remark that the number of entries per unit time, per unit area of investigation is higher than that of previous works based on a similar approach[1,4,7,47], which gives us confidence on the data set reliability.

Age histograms were generated to assess time variations of the magmatic activity (Fig. 1c and Supplementary Figs 1 and 4). The bin size for the histogram in Fig. 1c (that is, 0.3 Myr) was selected based on Scott's normal reference rule and the age measurement errors are in most cases smaller than or equal to this value (the analyses and conclusions hold if entries with age measurement error larger than this value or not provided are removed from the database). Histograms based on bin sizes of 0.2 and 0.4 Myr still show the peak of magmatism during the second half of the MSC (Supplementary Fig. 4). A histogram of data from a careful selection from the Earthchem archive (http://www.earthchem.org as of August 2016) throughout the Neogene in the Mediterranean (Supplementary Fig. 1) shows no other peaks comparable to that during the second half of the MSC, stressing the outstanding nature of this event. A histogram of data from a careful selection from the Earthchem archive (as of January 2017) throughout the 6.4–5 Ma time window worldwide shows no significant trends, which rules out global-scale forcings and indicates that the trends in Fig. 1c and Supplementary Fig. 1 are limited to the Mediterranean realm.

Exploring the magmatic effects of surface load variations. Overall, surface unloading, implying decreased lithostatic pressure at depth, enhances the production and emplacement/release of magma, whereas the opposite is true for surface loading. We provide hereafter more quantitative assessments as to the forcing from surface load changes on the production of magma by decompression partial mantle melting and the effects on magma reservoirs. In doing this, we account for the average relative position of the igneous provinces included in our database and salt deposits with respect to that of the basin (Fig. 1d).

Surface load changes and magma generation by decompression partial mantle melting. The magma production rate, DF/Dt, for pressure release melting at constant entropy, S, can be estimated as[2]:

$$\frac{DF}{Dt} = \left(\frac{\partial F}{\partial P}\right)_S \left(\frac{\partial P}{\partial t} - \bar{\mathbf{V}} \cdot \nabla P\right) \quad (3)$$

where F is the melt fraction, P is pressure, T is temperature, t is time and $\bar{\mathbf{V}}$ is the mantle velocity vector. At any given depth (that is, where the term $\partial F/\partial P$ is constant), a direct comparison between the terms $\partial P/\partial t$ and $\bar{\mathbf{V}} \cdot \nabla P$ provides a first-order assessment as to the potential relative contributions to the Mediterranean magmatism from MSC-related surface load variations and the background mantle upwelling, respectively.

Using the standard expression $P = \int \rho g \, dz$ to compute the lithostatic pressure at depth, z, and assuming a uniform rock density, ρ, of 3,000 kg m^{-3} and vertical component of $\bar{\mathbf{V}}$ in back-arc environments of up to a few centimetres per year[21], the term $\bar{\mathbf{V}} \cdot \nabla P$ varies on the order of hundreds of Pa yr^{-1}. With this in mind, we estimated $\partial P/\partial t$ due to MSC-related surface load variations, $\Delta L_{s(t)}$ (estimated as described in the previous section), solving the two-dimensional Stokes, continuity and advection equations using standard finite differences and marker-in-cell techniques on a regular grid using pressure–velocity formulations[49]. The Earth model is composed of two incompressible Maxwell viscoelastic layers (analogues for the crust and mantle) characterized by different viscosities, η_c and η_m, and elastic moduli, E_c and E_m, and with relative densities of 2,750 and 3,300 kg m^{-3}. The model domain (Fig. 2) measures 3,000 by 400 km in the horizontal and vertical dimensions, resolved by ~30 × 4 km element size and 160,000 markers advected accordingly to the computed velocity field and a fourth-order Runge–Kutta

scheme. Free-slip velocity boundary conditions are applied to all boundaries and an 8-km-thick 'sticky air' layer[49] is imposed at the top of the model domain. The upper layer is 50 km thick and characterized by a 6-km-thick basin-like structure on the right-hand side, whose density is varied through time to mimic a forcing comparable in magnitude and timing to $\Delta L_{s(t)}$ in Fig. 1b.

We tracked $\partial P/\partial t$ at a hypothetical magma source point located at ~60 km depth and in the proximity of (but outside) the basin-like structure (Fig. 2a), a choice driven by the fact that most rocks composing our database come from inland magmatic provinces (Fig. 1d). We found that, for common viscosities and elastic moduli[29], $\partial P/\partial t$ varies on the order of tens of Pa yr^{-1}, with peaks on the order of hundreds of Pa yr^{-1} if catastrophic events (for example, abrupt flooding of the Mediterranean at the end of the MSC) are involved. Higher $\partial P/\partial t$ values would be obtained if the hypothetical magma source point was shallower. These predictions are consistent with results from other studies[2,50] involved with surface load changes of different origins but similar magnitudes, which gives us confidence about the validity of the assumptions embedded in our model.

The modelling shows that, although $\partial P/\partial t$ at depth is in general one order of magnitude smaller than $\vec{\mathbf{V}} \cdot \nabla P$, it may reach up to similar values when extreme events occur (Fig. 2a–c). Following the analytical framework provided by ref. 5, and accordingly with equation (3), the adiabatic melt production rate due to mantle upwelling, Γ_{upw}, is:

$$\Gamma_{upw} = \rho_m V_y \left| \frac{dF}{dy} \right|$$

where y is a coordinate aligned with gravity and positive downwards and V_y is the vertical component of the mantle velocity vector. The volume of melts produced, Mv_{upw}, is obtained by depth integration of Γ_{upw}

$$Mv_{upw} = \int_{y_m}^{y_0} \Gamma_{upw}\, dy = \rho_m V_y \int_{y_m}^{y_0} \left| \frac{dF}{dy} \right| dy \quad (4)$$

where y_0 and y_m define the Earth's surface and the maximum depth at which partial melting occurs, respectively. The perturbation from $\Delta L_{s(t)}$ to Γ_{upw}, Γ_{sl}, can be calculated as:

$$\Gamma_{sl} = \frac{1}{g} \left| \frac{dF}{dy} \right| \frac{\partial P}{\partial t}$$

Let us define R such that:

$$R = \frac{\Gamma_{sl}}{\Gamma_{upw}} = \frac{1}{\rho_m g V_y} \left(\frac{\partial P}{\partial t} \right) \quad (5)$$

is the percentage modulation of Γ_{upw} due to $\Delta L_{s(t)}$. In Fig. 2b,c, we provide an estimate of R assuming uniform and constant $\rho_m = 3{,}300$ kg m^{-3} and $V_y = -1$ cm yr^{-1}. Note that, because negative V_y implies upwelling in our reference system, when $\Delta L_{s(t)}$ is positive R is negative and vice versa. In addition, under the assumption of uniform and constant V_y and ρ_m, R is solely controlled by $\partial P/\partial t$. The additional volume of melts produced due to $\Delta L_{s(t)}$, Mv_{sl}, is obtained by depth integration of Γ_{sl},

$$Mv_{sl} = \int_{y_m}^{y_0} \Gamma_{sl}\, dy = \frac{1}{g} \int_{y_m}^{y_0} \left| \frac{dF}{dy} \right| \frac{\partial P}{\partial t}\, dy \quad (6)$$

In Fig. 3, this theory is applied to an equilibrium continental geotherm and a parameterization for partial mantle melting as functions of pressure and temperature[26] to provide estimates of Γ_{upw}, Γ_{sl} and the additional magma per unit time and surface area produced during the unloading phase of the reference MSC scenario.

In general, $\partial P/\partial t$ values due to surface load variations are sustained for relatively short times outside surface loading/unloading phases because of the viscous stress relaxation. However, adiabatic loading/unloading implies instantaneous modifications of the magma production rates. Additional melts then upwell through the lithosphere at rates that may be as fast as tens of metres per year[29], and thus the newly produced magma can migrate through a 100-km-thick lithosphere in less than ~10 kyr. We conclude that substantial deviations from the surface or near-surface magmatic record by modulations of the background magma production rates due to MSC-related ΔL_s should be expected.

Surface load changes, overpressure of magma reservoirs and dyke formation. Ref. 3 derived an equation to investigate the effects of glacial unloading on the dynamics of dyke formation assuming that a crustal magma chamber is embedded into Maxwell viscoelastic wall rocks. We adapt this formulation to our work by substituting the rate of glacial unloading term with the rate of change of surface load due to the MSC, $\partial \Delta L_s/\partial t$, and obtain:

$$\frac{\partial \Delta P_{ch}}{\partial t} + \frac{E_c}{\eta_c} \Delta P_{ch} = -\frac{\partial \Delta L_s}{\partial t} \quad (7)$$

where $\Delta P_{ch} = P_{ch} - P$ is the overpressure within the magma chamber (with P_{ch} and P being the pressure within the magma chamber and the remote lithostatic stress, respectively), while E_c and η_c are the elastic modulus and viscosity of the crustal wall rock. We remark that the inherent simplifications into our geodynamic modelling prevent us from estimating P_{ch} and, therefore, the solution of equation (7) is beyond our possibilities. However, for very high η_c (for example, $\geq 10^{23}$ Pa s), the rate of change of surface load variations (rather than the absolute magnitude) essentially controls $\partial \Delta P_{ch}/\partial t$—that is equation (7) becomes:

$$\frac{\partial \Delta P_{ch}}{\partial t} = -\frac{\partial \Delta L_s}{\partial t} \quad (8)$$

Assuming that this condition applies to our geodynamic models, we use the computed $\partial P/\partial t$ as the forcing term in equation (8) (that is, we impose $-\partial \Delta L_s/\partial t = \partial P/\partial t$) and plot $\partial \Delta P_{ch}/\partial t$ at 20 km depth, above the reference point shown in Fig. 2. Results are shown in Fig. 4a and discussed in the main text. If the viscous response is not negligible (for example, for $\eta_c \leq 10^{22}$ Pa s), instead, E_c/η_c (that is, the inverse Maxwell relaxation timescale, $1/\tau_m$) with respect to the timescale at which surface load variations take place, τ_{Ls} (on the order of 10^4–10^5 yr for MSC-related events), defines the system response time. τ_m is estimated to be in the order of 10^4 kyr or shorter for silicic dyke formation and volcanism[3,29]. Assuming $\Delta P_{ch} > \Delta P_{max}$, where ΔP_{max} is the maximum sustainable magma chamber overpressure, and for τ_m/τ_{Ls} smaller than ~0.1, eruptions by dyke formation are expected with a delay of ~10 kyr after the forcing by surface load variations[3]—that is shorter than τ_{Ls}. As such, substantial deviations from the surface or near-surface magmatic record by modulations of the overpressure within magma chambers due to MSC-related ΔL_s should be expected.

Code availability. The code used for the geodynamic modelling and all related results can be requested directly from the leading author or accessed at https://sites.google.com/site/pietrosternai1/repositories/nature-geoscience-2017.

Data availability. The data used in this work, provided in Supplementary Table 1, is obtained from the Earthchem archive at http://www.earthchem.org and manual literature screening. The authors declare that all data supporting the findings of this study are available within the article and its Supplementary Information files.

References

35. Jolivet, L. & Faccenna, C. Mediterranean extension and the Africa–Eurasia collision. *Tectonics* **19,** 1095–1106 (2000).
36. Krijgsman, W. & Garcés, M. Paleomagnetic constraints on the geodynamic evolution of the Gibraltar Arc. *Terra Nova* **16,** 281–287 (2004).
37. Malinverno, A. & Ryan, W. B. Extension in the Tyrrhenian Sea and shortening in the Apennines as result of arc migration driven by sinking of the lithosphere. *Tectonics* **5,** 227–245 (1986).
38. Jolivet, L. *et al*. Subduction, convergence and the mode of backarc extension in the Mediterranean region. *Bull. Soc. Géol. Fr.* **179,** 525–550 (2008).
39. Duggen, S., Hoernle, K., Van Den Bogaard, P., Rüpke, L. & Morgan, J. P. Deep roots of the Messinian salinity crisis. *Nature* **422,** 602–606 (2003).
40. Pe-Piper, G. & Piper, D. J. *Postcollisional Tectonics and Magmatism in the Mediterranean Region and Asia* (eds Dilek, Y. & Pavlides, S.) 259–282 (Geological Society of America, 2006).
41. Jolivet, L. *et al*. The geological signature of a slab tear below the Aegean. *Tectonophysics* **659,** 166–182 (2015).
42. Sternai, P., Jolivet, L., Menant, A. & Gerya, T. Driving the upper plate surface deformation by slab rollback and mantle flow. *Earth Planet. Sci. Lett.* **405,** 110–118 (2014).
43. Menant, A., Sternai, P., Jolivet, L., Guillou-Frottier, L. & Gerya, T. V. 3D numerical assessments for mantle flow and magma genesis in laterally constrained subduction zones: the eastern Mediterranean case study. *Earth Planet. Sci. Lett.* **442,** 93–107 (2016).
44. Blanc, P. L. Of sills and straits: a quantitative assessment of the Messinian Salinity Crisis. *Deep Sea Res. Part I* **47,** 1429–1460 (2000).
45. Millero, F., Chen, C., Bradshaw, A. & Schleicher, K. A new high pressure equation of state for seawater. *Deep-Sea Res. A* **27,** 255–264 (1980).
46. Govers, R. Choking the Mediterranean to dehydration: the Messinian salinity crisis. *Geology* **37,** 167–170 (2009).
47. von Blanckenburg, F. & Huw Davies, J. Slab breakoff: a model for syncollisional magmatism and tectonics in the Alps. *Tectonics* **1,** 120–131 (1995).
48. McKenzie, N. R. *et al*. Continental arc volcanism as the principal driver of icehouse–greenhouse variability. *Science* **352,** 444–447 (2016).
49. Gerya, T. *Introduction to Numerical Geodynamic Modelling* (Cambridge Univ. Press, 2010).
50. Schmidt, P. *et al*. Effects of present-day deglaciation in Iceland on mantle melt production rates. *J. Geophys. Res.* **118,** 3366–3379 (2013).